

# Thermo, Electrical and Structural Properties of Solid Electrolyte Doped Bi<sub>2</sub>O<sub>3</sub> Binary and Ternary Systems

Erkan Erden<sup>a</sup>, Semra Durmuş Acer<sup>b\*</sup>

<sup>a</sup>Institute of Science, Kütahya Dumlupınar University, 43000 Kütahya, Turkey

<sup>b</sup>Department of Energy Systems Engineering, Faculty of Technology, Kütahya Dumlupınar University, 43500 Kütahya, Turkey

<sup>a</sup>Email: [semra.durmus@dpu.edu.tr](mailto:semra.durmus@dpu.edu.tr)

<sup>b</sup>Email: [erkan.erden@hotmail.com](mailto:erkan.erden@hotmail.com)

## Abstract

In this study; production and characterization of Bi<sub>2</sub>O<sub>3</sub> based solid electrolytes used in medium-temperature solid oxide fuel cells (IT-SOFC) were performed. Solid electrolyte samples were obtained using compounds Eu<sub>2</sub>O<sub>3</sub>, Dy<sub>2</sub>O<sub>3</sub> and Bi<sub>2</sub>O<sub>3</sub>. Stable phase which can create the highest power density  $\delta$ -Bi<sub>2</sub>O<sub>3</sub> (cubic-fcc) was tried to be reached for IT-SOFC. X-ray diffractometry (XRD) and differential thermal analysis and thermal gravimeter (TG/DTA) with binary (Eu<sub>2</sub>O<sub>3</sub>-Bi<sub>2</sub>O<sub>3</sub>) and ternary (Eu<sub>2</sub>O<sub>3</sub>-Dy<sub>2</sub>O<sub>3</sub>-Bi<sub>2</sub>O<sub>3</sub>) powder materials were analyzed for crystal structure identification. Bi<sub>2</sub>O<sub>3</sub>-based compounds with the cubic structure have been identified in those composition regions ((Bi<sub>2</sub>O<sub>3</sub>)<sub>0,6</sub>(Eu<sub>2</sub>O<sub>3</sub>)<sub>0,3</sub>) and ((Bi<sub>2</sub>O<sub>3</sub>)<sub>1-x-y</sub>(Dy<sub>2</sub>O<sub>3</sub>)<sub>x</sub>(Eu<sub>2</sub>O<sub>3</sub>)<sub>y</sub>, 0.25 ≤ x ≤ 0.35, y=0,05). Four point measurement techniques were used for electrical characterization. The conductivity of the ternary system is higher than the conductivity of the binary system. The highest conductive sample is (Bi<sub>2</sub>O<sub>3</sub>)<sub>0,7</sub>(Dy<sub>2</sub>O<sub>3</sub>)<sub>0,25</sub>(Eu<sub>2</sub>O<sub>3</sub>)<sub>0,05</sub> 0.3 S/cm at 800 °C.

**Keywords:** Bismuth trioxide (Bi<sub>2</sub>O<sub>3</sub>); Solid oxide electrolyte; Dysprosium trioxide (Dy<sub>2</sub>O<sub>3</sub>); Europium trioxide (Eu<sub>2</sub>O<sub>3</sub>); Oxygen ionic conduction.

## 1. Introduction

Fuel cells generate electricity by electrochemical means, such as accumulator and other batteries. Accumulator and batteries perform electrochemical cycles with the energy they store and provide electricity generation which have a short life.

-----  
\* Corresponding author.

Whereas, fuel cells; it generates electricity by electrochemical means as long as air and fuel inflow without stored energy. Because of these properties, they are also called “continuously working batteries” or “electrochemical machines [1-3]. They are also called “zero emission engines ile with their non-polluting properties. A simple fuel cell consists of a porous anode electrode and cathode electrode and electrolyte sandwiched in them. The porous structure is preferred because gas passages are better. Fuel is supplied to the anode (negative) electrode and oxidizer input to the cathode (positive) electrode. In general, it is preferred to use air or oxygen as the oxidizer and hydrogen as the fuel. An ideal electrolyte should first provide chemical or mechanical compatibility such as thermal expansion similarity with cathode, anode and other components in the fuel cell in which it is located, and not unnecessary reaction with components. Any interaction with other components is that the electrolyte loses its structural or crystallographic properties, which is undesirable in an ideal electrolyte [4,5]. The ideal electrolyte should retain its properties (conductivity, thermal, mechanical, chemical and crystallographic) over a long period of use [6-9]. It should also have a high level of ionic electrical conductivity. Oxygen ionic conduction mechanism in electrolytes is formed by the hopping mechanism movement to the empty  $O^{-2}$  lattice points of the  $O^{-2}$  ions which are driven by the effect of electric current and temperature [10-12]. The fact that this process is very frequent ensures that the amount of ionic electrical conduction, which is one of the characteristics of the ideal electrolyte mentioned above, is also high. Temperature is the most important factor in the jump of the  $O^{-2}$  ions in the neighboring empty point. They also need less than 1 eV of energy to move from one place to another in the crystal structure. It should not be forgotten that the electrolyte material used for oxygen ion conduction must have an oxygen molecule in its crystal structure. In the  $M_2O_x$  formula, the crystal structures can be stabilized by simulating fluorite structure by adding certain elements such as V, Sb, La, Pr, Nd, Sm, Eu, Gd, Tb, Dy instead of M doping, in essence is the process of ion exchange. In the doping process, lower valence cations are added to the compound to form oxygen gaps and increase the mobility and movement of oxygen ions. Thus, while the ionic conductivity of oxygen increases, it increases in electrical conductivity Thanks to the oxidized compounds added to pure  $Bi_2O_3$ , its unstable phases (e.g.  $\delta-Bi_2O_3$  phase) become stable for fuel cells at room temperature [13,14]. In present study, We have studied the formation stable phase of bismuth trioxide doped with europium trioxide binary systems  $((Bi_2O_3)_{1-x}(Eu_2O_3)_x)$  have been examined. It has been shown that the system contains  $Bi_2O_3$ -based solid solutions with cubic and monoclinic structures, depending on composition. Subsequent to, stable phase of bismuth trioxide doped with europium trioxide and dysprosium trioxide ternary systems  $((Bi_2O_3)_{1-x-y}(Dy_2O_3)_x(Eu_2O_3)_y)$  have been examined.

## 2. Material and methods

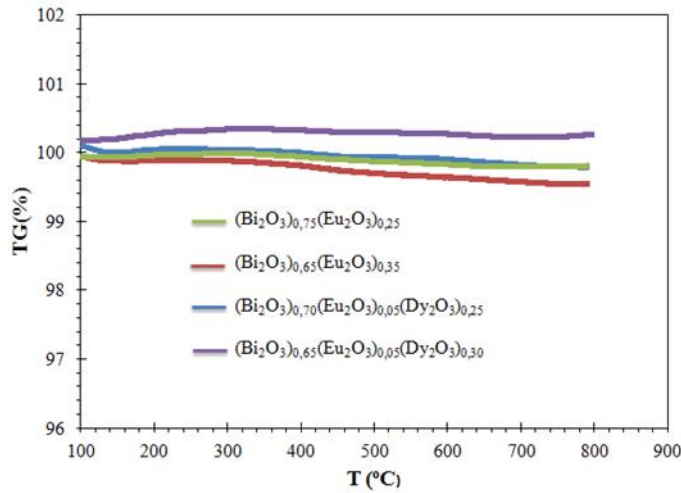
$(EuO_{1.5})_x-(BiO_{1.5})_{1-x}$  (xESB) and  $(DyO_{1.5})_x-(EuO_{1.5})_y-(BiO_{1.5})_{1-x-y}$  (xDyESB) combination were produced by solid-state synthesis. First, three different compositions were investigated:  $(EuO_{1.5})_x-(BiO_{1.5})_{1-x}$  (where  $x = 0.25, 0.30, 0.35$ ) These compositions are referred as 25ESB, 30ESB and 35ESB. Then, with the contribution of  $Dy_2O_3$ , ternary systems were produced. Different compositions with a fixed 5 mol %  $EuO_{1.5}$  doping concentration were prepared; these compositions are recall as 25D5ESB, 30D5ESB and 35D5ESB. The solid state reaction experimental process began with weighing the powders ( $Bi_2O_3$  (99.99% pure),  $Dy_2O_3$  (99.99% pure) and  $Eu_2O_3$  (99.99% pure)) at the predicted molar ratios. Since the triple systems are more stable and have higher electrical conductivity than the binary systems, the  $Dy_2O_3$ - $Eu_2O_3$ - $Bi_2O_3$  triple system was also prepared

after the  $\text{Eu}_2\text{O}_3\text{-Bi}_2\text{O}_3$  binary system. In the literature, 25% and greater contributions were made in the triple system due to obtaining stable phases in the  $\text{Dy}_2\text{O}_3\text{-Bi}_2\text{O}_3$  binary systems at around 25% [15]. The solid state reaction experimental process began with weighing the powders at the predicted molar ratios. Agate mortar was used to ensure homogeneity of the weighed binary and ternary system powders. The agate was ground in mortar for about 15 minutes. Binary systems were fired alumina pots at  $850^\circ\text{C}$  for 12 h and at  $800^\circ\text{C}$  for 48 h. Ternary systems were fired in alumina pots at  $750^\circ\text{C}$  for 48 h and at  $700^\circ\text{C}$  for 48 h. After heat treatment, XRD and TG / DTA measurements of binary and ternary systems were performed and electrical conductivity measurements as well as XRD and TG / DTA measurements were performed. For electrical conductivity measurements, heat treated samples were prepared with 0.5 mm thin and 13 mm diameter pallets. The structure of the crystal lattices was examined by XRD measurements and it was determined that it was single or multi-phase. The X-ray powder diffraction (XRD) data of the samples were recorded between  $10^\circ$  and  $70^\circ$ , by using AXSD8 Advance type diffractometer.  $\text{Cu-K}\alpha$  radiation was used for the determination of the crystal structure of the samples at room temperature. In the TG / DTA measurement system, TG and DTA measurements were taken simultaneously. Mass measurements of the binary and ternary systems from room temperature to high temperatures were controlled by TG measurements, while changes in crystal lattices were observed in the same temperature range with DTA measurements. The examples, generally 20 mg in mass, were fired to  $800^\circ\text{C}$  at a heating rate of  $200^\circ\text{C min}^{-1}$ , and then cooled to room temperature. Measurements were made in a dynamic air atmosphere by using a platinum sample holder and an inert  $\alpha\text{-Al}_2\text{O}_3$  reference substance. Four point conductivity measurement method was used to determine the electrical conductivity characteristics of the samples. For this measurement, Keithley 2700 brand equipment and equipment in Erciyes University Research Laboratory were used. Special conductive adhesive was not used for the contact or fixation of the sample. Using the temperature change programmable furnace, the programmed temperatures are reached automatically with a constant heating speed at certain times. The samples were kept in place in the furnace and were not displaced throughout the measurements. After providing reliable contact of platinum terminals on the tablets placed in the conductivity measurement kit, voltage was applied between the power supply and connections 1 and 4. measurements were performed with DAQ (Data Acquisition) control system. The collected data were processed with Keithley Integra Up & Running software on the scanner card which is part of the system for electrical conductivity measurement. The values sent from the multimeter at specific intervals were graphed with ExcelINX programming language.

### 3. Results

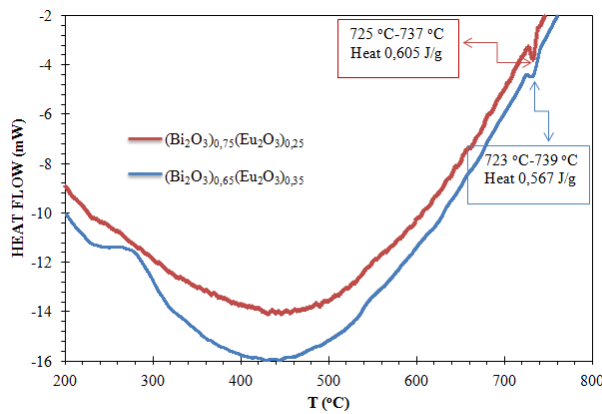
Figure 1 shows the TG curves of polycrystalline  $((\text{EuO}_{1.5})_x\text{-(BiO}_{1.5})_{1-x})$  (xESB) and  $((\text{DyO}_{1.5})_x\text{-(EuO}_{1.5})_y\text{-(BiO}_{1.5})_{1-x-y})$  xDyESB samples. When the TG curve is considered, the mass loss resulting from the processes up to  $800^\circ\text{C}$  is considered to be  $\sim 3\%$ , which is negligible.

Figure 2 and Figure 3 shows the DTA curves of polycrystalline  $((\text{EuO}_{1.5})_x\text{-(BiO}_{1.5})_{1-x})$  (xESB) and  $((\text{DyO}_{1.5})_x\text{-(EuO}_{1.5})_y\text{-(BiO}_{1.5})_{1-x-y})$  xDyESB samples, respectively. Figure 2 shows that endothermic and/or exothermic peaks were also observed in the DTA curve of the mixed phase. In the DTA heating curves of the mixed phase samples, the two endothermic peaks correspond to the from  $\square\square$  to  $\square$  ( $600\text{-}650^\circ\text{C}$ ) and from  $\square\square$  to  $\square\square$  ( $690\text{-}750^\circ\text{C}$ ) structural phase transitions.



**Figure 1:** TG curves of the  $(\text{EuO}_{1.5})_x-(\text{BiO}_{1.5})_{1-x}$  and  $(\text{DyO}_{1.5})_x-(\text{EuO}_{1.5})_y-(\text{BiO}_{1.5})_{1-x-y}$  samples.

During heating, only one phase transition, from  $\square\square$  to  $\square$ , is observed [16]. The phase transition in the 25ESB sample was shown as an endothermic peak with a heat release of 0.605 J / g in the temperature range of 725 °C to 737 °C. Similarly, in the 30ESB sample, 723 °C - 739 °C, 0,567 J / g.  $(\text{DyO}_{1.5})_x-(\text{EuO}_{1.5})_y-(\text{BiO}_{1.5})_{1-x-y}$  samples are similar in polymorphism (Figure 3). When the DTA curve is observed in Figure 3, no endothermic or exothermic peak is observed. Due to the high thermal stability of these samples, it was found to be highly compatible with the XRD pattern. Because a stable homogeneous phase ( $\delta$ -phase) was obtained in XRD results. The other  $\delta$ -phase observed in the sample produced similar results from DTA.



**Figure 2:** DTA curves of  $(\text{EuO}_{1.5})_x-(\text{BiO}_{1.5})_{1-x}$  metastable samples with europium content,  $\square\square\square\square$  phase, heating.

Figure 4 and Figure 5 shows powder XRD patterns of polycrystalline  $(\text{EuO}_{1.5})_x-(\text{BiO}_{1.5})_{1-x}$  samples heat-treated 800°C 48 h and 850°C 12 h, respectively. The XRD spectra of all samples were very similar to each other. Peaks belonging to the binary phase are marked as shown in the overlaps. Binary phases, which are the cause of the endothermic peaks seen in the DTA results of ESB series, also appear in XRD spectra [16]. The peaks of the stable phases were compared. Stable phases could not be obtained from ESB series. In addition, the QualX

program provides control of the phases.

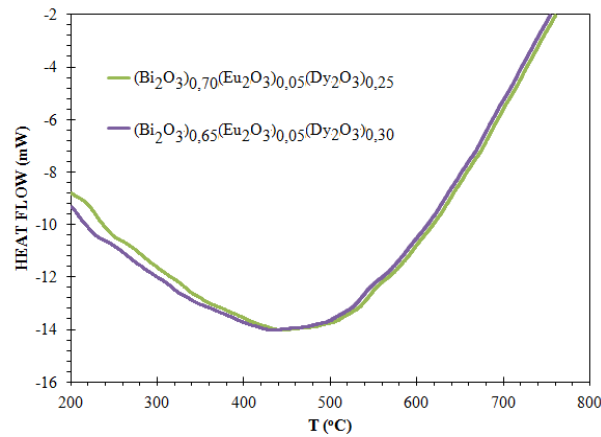


**Figure 3:** DTA curves of  $(\text{DyO}_{1.5})_x-(\text{EuO}_{1.5})_y-(\text{BiO}_{1.5})_{1-x-y}$  cubic samples with dysprosium trioxide content  $\square\square\square$  phase, heating.

As a result of the program, all these materials crystallize in a rhombohedral symmetry and their average crystal structure was described with a hexagonal cell in  $R3m$  space group [17-18]. Based on the reals that  $\text{Eu}^{2+}$  (1.17 Å) is much larger than  $\text{Bi}^{3+}$  (1.03 Å), it can be concluded that the rhombohedral phase is rich in  $\text{Eu}^{2+}$  content. Therefore, a triple system was obtained by selecting  $\text{Dy}^{2+}$  (1.07 Å) with an ionic radius close to  $\text{Bi}^{3+}$  (1.03 Å), and reducing the amount of Eu [19].

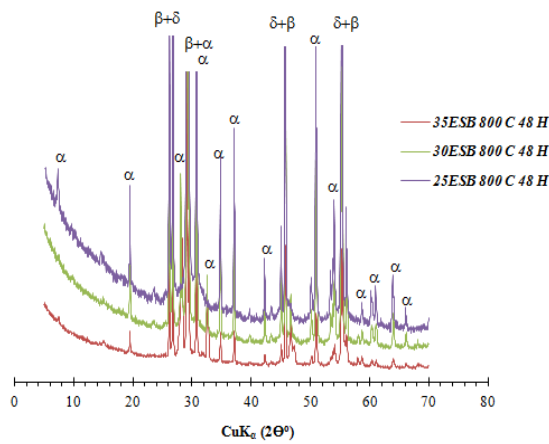


**Figure 4:** Powder XRD patterns of the polycrystalline  $(\text{EuO}_{1.5})_x-(\text{BiO}_{1.5})_{1-x}$  samples,  $\square\square\square$  phase, heat treated 800°C and 48H

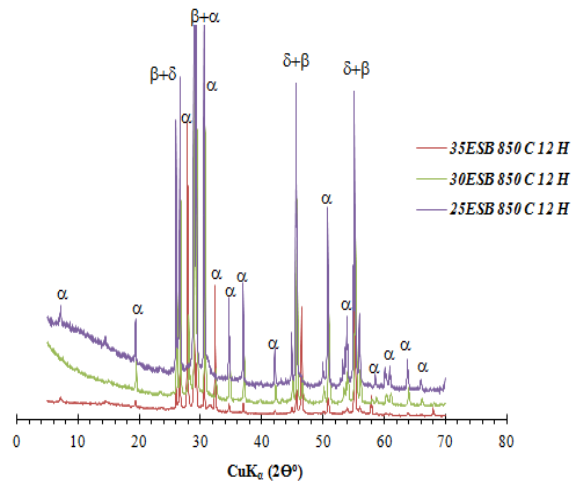


**Figure 5:** Powder XRD patterns of the polycrystalline  $(\text{EuO}_{1.5})_x-(\text{BiO}_{1.5})_{1-x}$  samples,  $\square\square\square\square$  phase, heat treated  $850^\circ\text{C}$  and 12H

Figure 6 and Figure 7 shows powder XRD patterns of polycrystalline  $((\text{DyO}_{1.5})_x-(\text{EuO}_{1.5})_y-(\text{BiO}_{1.5})_{1-x-y})$  samples heat-treated  $700^\circ\text{C}$  48 h and  $750^\circ\text{C}$  48 h, respectively. According to ESB series, DyESB series gave very positive results. Because the majority of the peaks of the binary phase are lost and tend to be stable phase is very high. Peaks with single phase are marked. And this phase is one of the most stable phases of  $\text{Bi}_2\text{O}_3$  cubic phase ( $\square\square\text{Bi}_2\text{O}_3$ ) and is the ideal phase for solid oxide fuel cells. Unlike ESB, the addition of  $\text{Dy}_2\text{O}_3$  increased the tendency to be electrolyte. Since the ionic radius of  $\text{Dy}^{2+}$  ( $1.07 \text{ \AA}$ ) is close to  $\text{Bi}^{3+}$  ( $1.03 \text{ \AA}$ ), and the amount of additive of  $\text{Dy}^{2+}$  is rich, DyESB system is stable phase. Furthermore, the DTA data of the DyESB series proved to be a single phase. Because no endothermic or exothermic reaction took place. XRD spectra show some impurity peaks as well as severe peaks. They have been neglected. Other thermal and electrical conductivity results support  $\square\text{-Bi}_2\text{O}_3$ .

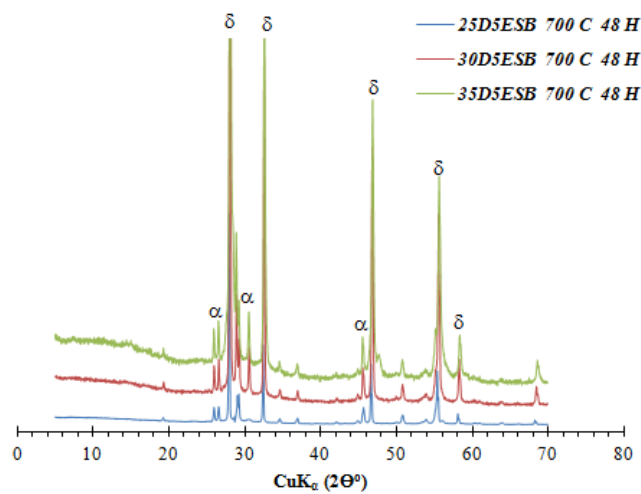


**Figure 6:** Powder XRD patterns of the polycrystalline  $((\text{DyO}_{1.5})_x-(\text{EuO}_{1.5})_y-(\text{BiO}_{1.5})_{1-x-y})$  samples  $\square\square\square\square$  phase, heat treated  $700^\circ\text{C}$  and 48H

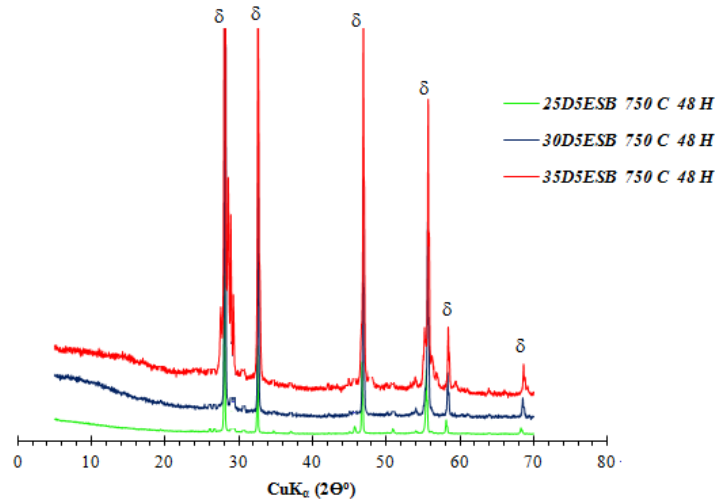


**Figure 7:** Powder XRD patterns of the polycrystalline  $((\text{DyO}_{1.5})_x-(\text{EuO}_{1.5})_y-(\text{BiO}_{1.5})_{1-x-y})$  samples  $\square\square\square\square$  phase, heat treated  $750^\circ\text{C}$  and 48H

Because the ionic radii of the material doped into the crystal are different from Bi, it affects the lattice parameters and the lattice tension. As the contribution rate increases, the crystal oxygen gaps increase and the crystal grows. With the increase of oxygen gaps, the knitting defect and thus the knitting tension ratio increases. Temperature dependent electrical conductivity graphs of the samples are shown in Figure 8-10. Operating temperatures of medium temperature fuel cells are generally seen as  $650\text{-}850^\circ\text{C}$  in literature surveys [20-23]. When evaluating the electrical conductivity data of our study, the working temperature is  $\sim 670\text{-}680^\circ\text{C}$ . When the electrical conductivity graphs of the solid electrolytes produced in the binary system  $(\text{Eu}_2\text{O}_3)_x(\text{Bi}_2\text{O}_3)_{1-x}$  with a molar contribution ratio of  $0.25 \leq x \leq 0.35$  were evaluated, the highest electrical conductivity value of 0.25 mol Eu doped E25B ( $T = 677^\circ\text{C}$ ,  $\square\square = 4.52 \Omega^{-1}\text{cm}^{-1}$ ). Then, respectively, 0.35 mol Eu doped E35B ( $T = 672^\circ\text{C}$ ,  $\square\square = 2.51 \Omega^{-1}\text{cm}^{-1}$ ), 0.30 mol Eu doped E30B ( $T = 664^\circ\text{C}$ ,  $\square\square\square = 2.44 \Omega^{-1}\text{cm}^{-1}$ ). In the binary system, electrical conductivity measurements at  $850^\circ\text{C}$  were not repeated due to the multiplicity of unstable phases.

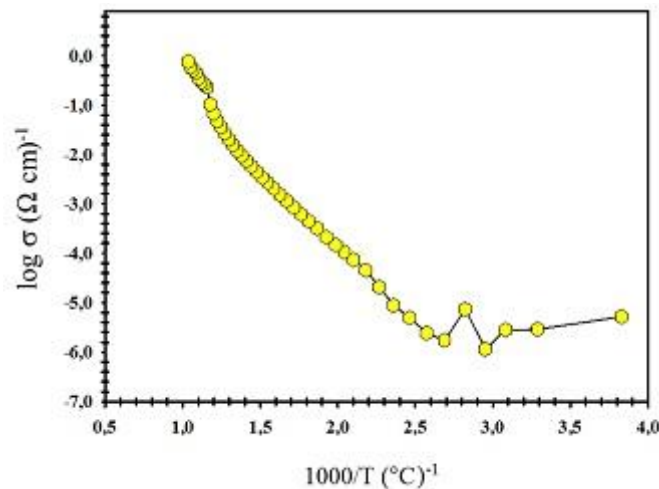


**Figure 8:** Electrical conductivity diagram after  $800^\circ\text{C}$  48 hours heat treatment for E25B sample.

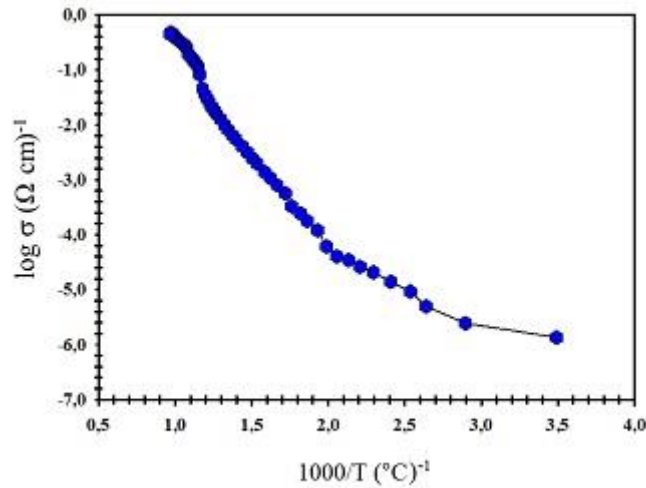


**Figure 9:** Electrical conductivity diagram after 800°C 48 hours heat treatment for E30B sample.

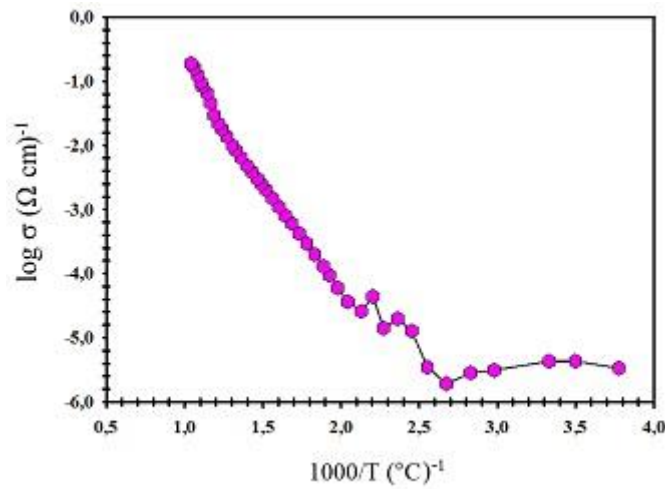


**Figure 10:** Electrical conductivity diagram after 800°C 48 hours heat treatment for E35B sample.

The electrical conductivity graphs at 800 °C support the XRD results and show that there is no homogeneous phase. They are sudden changes in slopes because there are transitions from one phase to another. Transitions from tetragonal  $\square\square\square\square$  phase to cubic phase are observed in all graphs, especially at high temperatures. Temperature dependent electrical conductivity graphs of the ternary system sample are shown in Figure 11.

Combined electrical conductivity graphs are shown because others are very similar (Figure 12 and Figure 13). The slope changes caused by sudden fractures at certain temperatures seen in the electrical conductivity measurement graphs of our samples consisting of double and triple systems gave information that the conductivity mechanism has changed or the crystal structure has changed. Again, the sudden changes in the slopes where the existing phase changes of ESB in the binary system were observed in the electrolyte of E5D25B in the triple system.

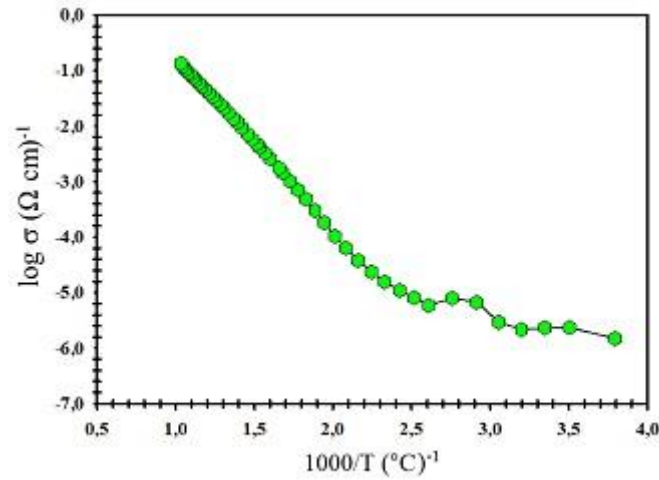


Figure 11: Electrical conductivity diagram after 750°C 48 hours heat treatment for E5D25B sample

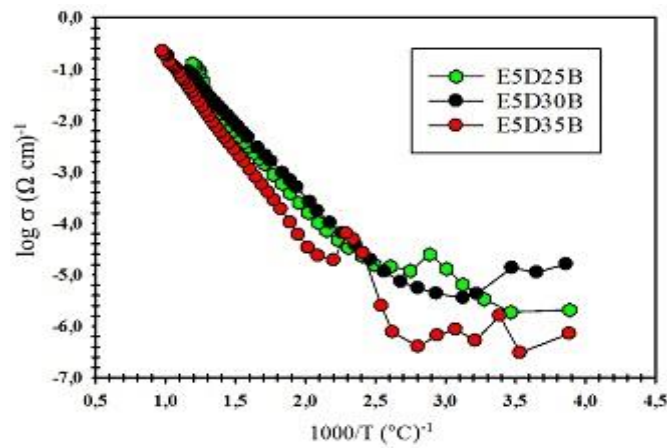


Figure 12: Electrical conductivity comparisons of samples which 700°C 48 hours heat treated

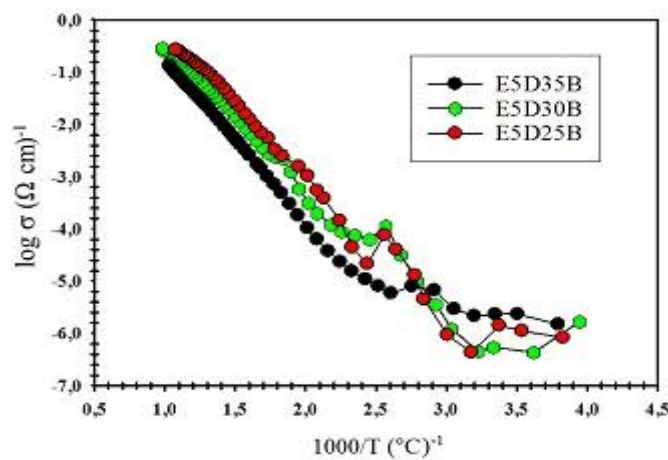
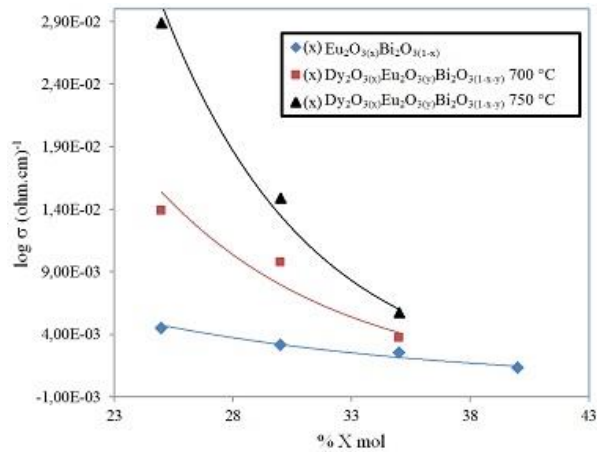


Figure 13: Electrical conductivity comparisons of samples which 750°C 48 hours heat treated

Because, when we look at the XRD graphs of this electrolyte, we can see the peaks of the binary phase. The electrical conductivity values of the binary and triple systems measured at 670 ° C were compared (Figure 14). As can be seen in the graph, while the conductivity values obtained from the binary system are low, the conductivity values obtained from the triple system are high. A higher conductive value is seen in the samples with a triple system with a heat treatment temperature of 750 ° C. Electrolyte sample which could not be obtained by binary system was obtained by triple system with low sintering temperature. Stable phases and high conductive electrolyte samples could be obtained due to the difference in ion radius and diffusion rate of Dy according to Eu element.



**Figure 14:** Electrical conductivity comparisons of samples which binary systems and triple systems

As is known, the electrical conductivity is related to the load carrier. Thus, the  $E_a$  value refers to the energy of activation or threshold energy, which is the energy for the load carriers to pass from one cavity to the other cavities. The temperature dependence of ionic conductivity can be expressed by the following empirical equation:

$$\sigma_T = A \exp(-E_a/kT) \quad (1)$$

where  $r$  is the oxygen-ion conductivity,  $A$  is a pre-exponential constant,  $T$  is the absolute temperature,  $k$  is the Boltzmann constant and  $E_a$  is the activation energy for oxygen migration. Therefore, activation energy and pre-exponential terms are crucial determinants of the ionic conductivity of a solid [24]. The activation energy value of our binary system compound;  $0,61 \leq E_a$  değişim varies between 0,68 and our triple compound varies between  $0,56 \leq E_a \leq 0,62$ . The rate of change in these data is below the standard 1 eV. When the activation energy data are considered, it is seen that the values obtained in the binary system are higher than those obtained from the triple system. This corresponds to the electrical conductivity values indicated in Figure 14. The triple system with very high conductivity was found to have the lowest activation energies of samples with a heat treatment temperature of 750 ° C.

#### 4. Conclusion

XRD, TG / DTA and four point electrical conductivity measurements of solid electrolyte samples xESB

$((\text{EuO}_{1.5})_x-(\text{BiO}_{1.5})_{1-x})$  and  $x\text{DyESB } ((\text{DyO}_{1.5})_x-(\text{EuO}_{1.5})_y-(\text{BiO}_{1.5})_{1-x-y})$  were made. The cubic phase ( $\square\square\text{Bi}_2\text{O}_3$ ) was obtained more by the addition of the element  $\text{Dy}_2\text{O}_3$ . Since the ionic radius of  $\text{Eu}_2\text{O}_3$  was larger, the diffusion rate was lower, so no stable phases were formed. The solid electrolytes in the  $x\text{DyESB}$  series obtained by this study are among the electrolytes with high conductivity at medium temperatures as in the literature. The highest conductivity value obtained in this study is the heat treated 25D5ESB solid electrolyte at  $750^\circ\text{C}$  and its value is  $2.89 \times 10^{-2}$  at  $670^\circ\text{C}$  and  $0.582\text{ eV}$  for activation energy. This sample also has the lowest activation energy which is calculated by using the Arrhenius equation (1). As consequences of these results, we found that these materials can be used as electrolyte, especially in SOFCs, due to their high oxygen ion conductivity and structural stability properties.

## 5. Recommendations

- The electrical conductivity and strength of stable solid electrolytes can be increased by using nanoscale particles.
- Thin film of solid electrolytes can be studied.
- Cathode supported or anode supported cells can be prepared and cell performance can be evaluated.

## Acknowledgements

Authors would like to thank Kütahya Dumlupınar University's Research Fund for financially supported (Project no: 2015 - 74).

## References

- [1]. A. Boudghene Stambouli and E. Traversa, "Solid oxide fuel cells (SOFCs): a review of an environmentally clean and efficient source of energy," *Renew. Sust. Energy Rev.*, vol.6 p.433, 2002.
- [2]. E.J. Naimaster, A.K.Sleiti, "Potential of SOFC CHP systems for energy-efficient commercial buildings," *Energy and Buildings*, vol.61, p.153–160, 2013.
- [3]. A. Choudhury, H. Chandra and Arora A, "Application of solid oxide fuel cell technology for power generation—A review," *Renew. Sust. Energy Rev.*, vol.20, p.430-442, 2013.
- [4]. N. M. Sammes, G. A. Tompsett, H. Nafe and F. Aldingera, "Bismuth Based Oxide Electrolytes-Structure and Ionic Conductivity." *J. Eur. Ceram. Soc.*, vol.19, p.1801-1826, 1999.
- [5]. N.Jaiswal, K. Tanwar, R. Suman, D. Kumar, S. Upadhyay, O. Parkash, "A brief review on ceria based solid electrolytes for solid oxide fuel cells," *J. Alloys Compd.*, vol.781, p. 984-1005, 2019.
- [6]. E.P. Kharitonova, E.I. Orlova, N.V. Gorshkov, V.G. Goffman, S.A. Chernyak, V.I. Voronkova, "Polymorphism and conductivity of  $\text{Bi}_2\text{O}_3$ -based fluorite-like compounds in  $\text{Bi}_2\text{O}_3$ - $\text{Nd}_2\text{O}_3$ - $\text{MoO}_3$  system," *J. Alloys Compd.*, vol.787, p. 452-462, 2019.
- [7]. A.Watanabe, M.Sekita, "Stabilized  $\gamma$ - $\text{Bi}_2\text{O}_3$  phase in the system  $\text{Bi}_2\text{O}_3$ - $\text{Er}_2\text{O}_3$ - $\text{WO}_3$  and its oxide-ion conduction," *Solid State Ion.*, Vol. 176, p. 2429 – 2433, 2005.
- [8]. H. Sun, X. Guo, F. Yu, Z. Yang, G. Li, J. Li, H. Ding, F. Meng, Z. Fan, P. Wang, W. Yan, Z. Hu, "Enhanced sinterability and electrical performance of  $\text{Sm}_2\text{O}_3$  doped  $\text{CeO}_2/\text{BaCeO}_3$  electrolytes for intermediate-temperature solid oxide fuel cells through  $\text{Bi}_2\text{O}_3$  co-doping," *Ceram. Int.*, vol.45, p.

7667, 2019.

- [9]. İ.
- [10]. Ermiş, S.P.S. Shaikh, “Study of crystallographic, thermal and electrical properties of  $(\text{Bi}_2\text{O}_3)_{1-x-y}(\text{Tb}_4\text{O}_7)_x(\text{Gd}_2\text{O}_3)_y$  electrolyte for SOFC application,” *Ceram. Int.*, vol.44, p.18776, 2018.
- [11]. N. Jiang, E. D. Wachsman, S.H. Jung, “A higher conductivity  $\text{Bi}_2\text{O}_3$ -based electrolyte,” *Solid State Ion.*, vol.150, p.347, 2002.
- [12]. M. Arı, M. Balçı, Y. Polat, “Synthesis and characterization of  $(\text{Bi}_2\text{O}_3)_{1-x-y-z}(\text{Gd}_2\text{O}_3)_x(\text{Sm}_2\text{O}_3)_y(\text{Eu}_2\text{O}_3)_z$  quaternary solid solutions for solid oxide fuel cell,” *Chinese J. Phys.*, Vol.56, p. 2958-2966, 2018.
- [13]. İ. Ermiş, M. Arı, S.Durmuş Acer, Y. Dağdemir, “Phase stability and electric conductivity of  $\text{Eu}_2\text{O}_3$ - $\text{Tb}_4\text{O}_7$  co-doped  $\text{Bi}_2\text{O}_3$  electrolyte,” *Int. J. Hydrogen Energ.*, Vol.40, p.9485-9490, 2015.
- [14]. G. Malmros, “The Crystal Structure of alpha- $\text{Bi}_2\text{O}_3$ ,” *Acta Chem. Scand.*, vol.24, p.384, 1970.
- [15]. C.M.B. Hincapié, M.J.P. Cardenas, J.E.A. Orjuela, E.R. Parra and J.J.O. Florez, “Physical-chemical properties of bismuth and bismuth oxides: Synthesis,” *DYNA*, vol.79, p.139, 2012.
- [16]. R. Li, Q. Zhen, M. Drache, A. Rubbens, R.N.Vannier, “Preparation mechanism of  $(\text{Bi}_2\text{O}_3)_{0.75}(\text{Dy}_2\text{O}_3)_{0.25}$  nano-crystalline solid electrolyte,” *J. Alloys Compd.*, p. 446-450, 2010.
- [17]. E.P. Kharitonova, V.I. Voronkova, D.A. Belov, and E.I. Orlova, “Fluorite-like compounds with high anionic conductivity in  $\text{Nd}_2\text{MoO}_6$  e  $\text{Bi}_2\text{O}_3$  system,” *Int. J. Hydrogen Energy*, vol.41, p.10053, 2016.
- [18]. S. Obbade, M. Huve, E. Suard, M. Drache and P. Conflan, “Powder Neutron Diffraction and TEM Investigations of  $\text{Bi}_{0.775}\text{Ln}_{0.225}\text{O}_{1.5}$  Oxide Conductors (Ln=La, Pr, Nd, Sm, Tb, Dy) with Rhombohedral Bi-Sr-O type: Structural Relationships with Monoclinic  $\epsilon\text{-Bi}_{4.86}\text{La}_{1.14}\text{O}_9$  Form,” *J. Solid State Chem.*, vol.168,p. 91,2002.
- [19]. M. Drache, S.Obbade, J. P.Wignacourt and P. Conflant, “Structural and Conductivity Properties of  $\text{Bi}_{0.775}\text{Ln}_{0.225}\text{O}_{1.5}$  Oxide Conductors (Ln=La, Pr, Nd, Sm, Eu, Gd, Tb, Dy) with Rhombohedral Bi-Sr-O Type,” *J. Solid State Chem.*, vol.142, p.349, 1999.
- [20]. S. F. Wang, Y. F. Hsu, W. C. Tsai and H. C. Lu, “The phase stability and electrical conductivity of  $\text{Bi}_2\text{O}_3$ ceramics stabilized by Co-dopants,”*J. Power Sources*, vol.218, p.106-112, 2012.
- [21]. J. Dempsey, “Hydrogen Fuel Cell Engines and Related Technologies,” *Energy Technology Training Center*, USA, 2001.
- [22]. B. Timurkutluk, *Performance Analysis of an Intermediate Temperature Solid Oxide Fuel Cell*, Middle East Technical University, TURKEY, 2007.
- [23]. H. A. Taroco, J. A. F. Santos, R. Z. Domingues and T. Matencio, *Advances in Ceramics Synthesis and Characterization, Processing and Specific Applications*, CROITA, 2011.
- [24]. E. Yiğit, *The production and characterization of the solid oxide fuel cell with NiO composite anode,  $\delta\text{-Bi}_2\text{O}_3$  solid electrolyte and Inf cathode Thesis*, Erciyes University, TURKEY, 2014.
- [25]. D. W. Jung, K. L. Duncan and E. D. Wachsman, “Effect of total dopant concentration and dopant ratio on conductivity of  $(\text{DyO}_{1.5})_x(\text{WO}_3)_y(\text{BiO}_{1.5})_{1-x-y}$ ,” *Acta Mater.* vol.58, p.355, 2010.